Chapter 3. Experimental

3.1 Molecular Characteristics

A series of three ethylene/α-olefin copolymers - Ethylene/1-Butene (EB), Ethylene/1-Pentene (EP) and Ethylene/1-Hexene (EH) - with different lengths of branches (ethyl to *n*-butyl) and comonomer contents ranging from 0 to 16 mole % were used in the present study. These homogeneous copolymers made using constrained geometry metallocene catalysts (INSITE™ technology) were supplied by The Dow Chemical Co. They possess uniform distributions of branches in the different polymer chains and exhibit a rather narrow molecular weight distribution ($M_w/M_n \sim 2.0$). These features are in sharp contrast to Ziegler-Natta based systems,[1,2,3] wherein different polymer chains contain substantially different amounts of comonomer, and may be of markedly different molecular mass. The molecular characteristics of the copolymers provided by the supplier are listed in Table 1. The samples are designated by the acronym for the branch type followed by a number representing their macroscopic density (in g/ml). For example, EB-912 stands for an ethylene/1-butene copolymer whose density is 0.912 g/ml. The densities indicated are those provided by the supplier. The macroscopic density was also measured in our laboratory by Mr. L. Richardson, using a density gradient column. The experimental details are provided in a later section of this chapter. All the copolymers were received in the form of pellets and were subsequently melt pressed (at 160°C) into films of *ca*. 1mm thickness under nitrogen atmosphere. A Carver press was used for this purpose at a force of 1 metric ton.

Table 1 Molecular Characteristics of Ethylene/1-Butene (EB), Ethylene/1-Pentene (EP) and Ethylene/1-Hexene (EH) copolymers

Sample	M_w (g/mol.)	M_w/M_n	Mole % 1-Butene
EB928	99,800	2.04	1.45
EB912	105,300	1.95	4.61
EB894	93,900	2.08	8.97
EB883	103,200	1.98	12.6
EB879	103,000	2.00	13.7
EB874	99,800	2.04	15.8

Sample	M_w (g/mol.)	M_w/M_n	Mole % 1-Pentene
EP910	81,200	2.20	4.44
EP870	111,200	2.12	14.31

Sample	M_w (g/mol.)	M_w/M_n	Mole % 1-Hexene
EH910	85,400	2.03	3.60
EH886	101,600	2.14	10.70
EH869	133,500	2.01	14.20

3.2 ^{13}C NMR Spectroscopy

This technique was used to determine the copolymerization statistics of the copolymers. In addition, the number of branches per 1000 backbone carbon atoms and the mole percent of branches in each copolymer were obtained from the results of the ^{13}C NMR studies. Copolymer solutions were prepared by adding *ca.* 300 mg of the copolymer to 3 ml of 1,2,4-trichlorobenzene in a 15mm NMR tube. Such high concentrations were necessary in order to obtain reasonable signal-to-noise ratios. The NMR tubes were then sealed, heated up to 120°C and maintained at that temperature for 20 min. to ensure complete dissolution.

The NMR experiments were conducted on a 400MHz Varian FT-NMR instrument at 125°C with a frequency of 100.578 MHz under proton-decoupling conditions. The decoupler was gated on during data acquisition and off during the delay time. The choice of pulse sequence was made based on the requirement that the delay time be at least five times the spin-lattice relaxation time (T_1) to ensure 99% relaxation. Since T_1 for the methyl, methine and methylene carbons in 1,2,4-trichlorobenzene at 118°C are equal to 2.1, 2.3 and 1.3 seconds respectively[4,5], the pulse width and relaxation delay time were chosen at 14 and 10 seconds respectively. The data acquisition time was kept at 1.12 seconds, with 540 to 600 repetitions acquired for attaining adequate signal-to-noise ratios. Typical data acquisition times ranged between 1.5 and 2 hours. The peak assignments were made on the basis of previous studies on ethylene copolymers.[6,7,8,9,10,11]

3.3 Differential Scanning Calorimetry (DSC)

A series of heating, cooling and isothermal experiments were carried out on a Perkin Elmer DSC-2 calorimeter operated under dry nitrogen purge with a dry ice-isopropanol heat sink. Sample masses between 3 and 5 mg were utilized. There was no noticeable effect of sample mass on the results of the thermal analysis experiments, within this range of sample masses. Temperature calibration for heating scans was done using indium (Melting point = 156.61°C) and for cooling scans using *p*-azoxyanisole, a liquid crystalline material with an isotropic-nematic transition at 136°C. The three sets of experiments are described below:

1. Cooling at different rates from the melt (5, 10 and 20°C/min.)
2. Isothermal crystallization at room temperature (T_x = RT ~ 20°C) and
3. Isothermal crystallization at temperatures above room temperature.

Absolute heat capacities were evaluated from the data collected after appropriate baseline subtraction and calibration with a sapphire standard. Degrees of crystallinity, χ_c, were obtained from the experimentally observed heat of fusion, ΔH_{obsd}, using the following relationship,

$$(1) \qquad \chi_c = \frac{\Delta H_{obsd}}{\Delta H_0}$$

where ΔH_0 = the heat of fusion of completely crystalline linear PE (69 cal/g).[12,13]

The χ_c values in the present study were primarily evaluated from cooling scans rather than from heating scans. The crystallinities developed during isothermal crystallization at various temperatures were however obtained from the heating traces. The determination of χ_c from cooling scans eliminates any ambiguities regarding melting/re-crystallization/remelting or annealing during heating, since no such reorganization can occur during cooling. The details of the analysis of the calorimetric data are discussed

below. The assumptions and approximations involved with the analysis and the interpretation of this data are presented in a following section.

3.3.1 Determination of Heat Capacities and Degrees of Crystallinity

Absolute heat capacities were determined from the DSC thermograms, thereby allowing an accurate estimation of the degree of crystallinity of the samples as a function of temperature. The procedure adopted in this determination is outlined below, with an example.

Step 1. The crystallization of a sample on cooling from the melt (180°C) to -40°C at different rates ranging from 5 to 20°C/min was followed by recording the DSC thermogram during the cooling process. In addition, isotherms were collected at the beginning and end of the cooling process so that appropriate baseline corrections could be made to the sample scan. A corresponding set of baseline and sapphire scans was also collected under the same conditions and with the same run parameters.

Step 2. The straight line between the beginning and ending isotherms was constructed for each of the baseline, sapphire and sample scans. The respective displacements were estimated as the difference between the heat flow corresponding to the experimental scan (baseline (BD), sapphire (SaD) or sample (SmD)) and the straight line as shown in Figure 1.

Step 3. The displacement of the baseline, BD was subtracted from those of the sample (SmD) and sapphire (SaD) standard to yield the effective displacements of the sample, D_p^{sample} and that of sapphire, $D_p^{sapphire}$, respectively. The absolute heat capacities, $C_p(T)$ of the sample were calculated from these effective displacements using the equation,

$$C_p(\text{sample}) = \frac{W_{\text{sapphire}}}{W_{\text{sample}}} \times \frac{D_p^{sample}}{D_p^{sapphire}} \times C_p^{sapphire} \qquad (2)$$

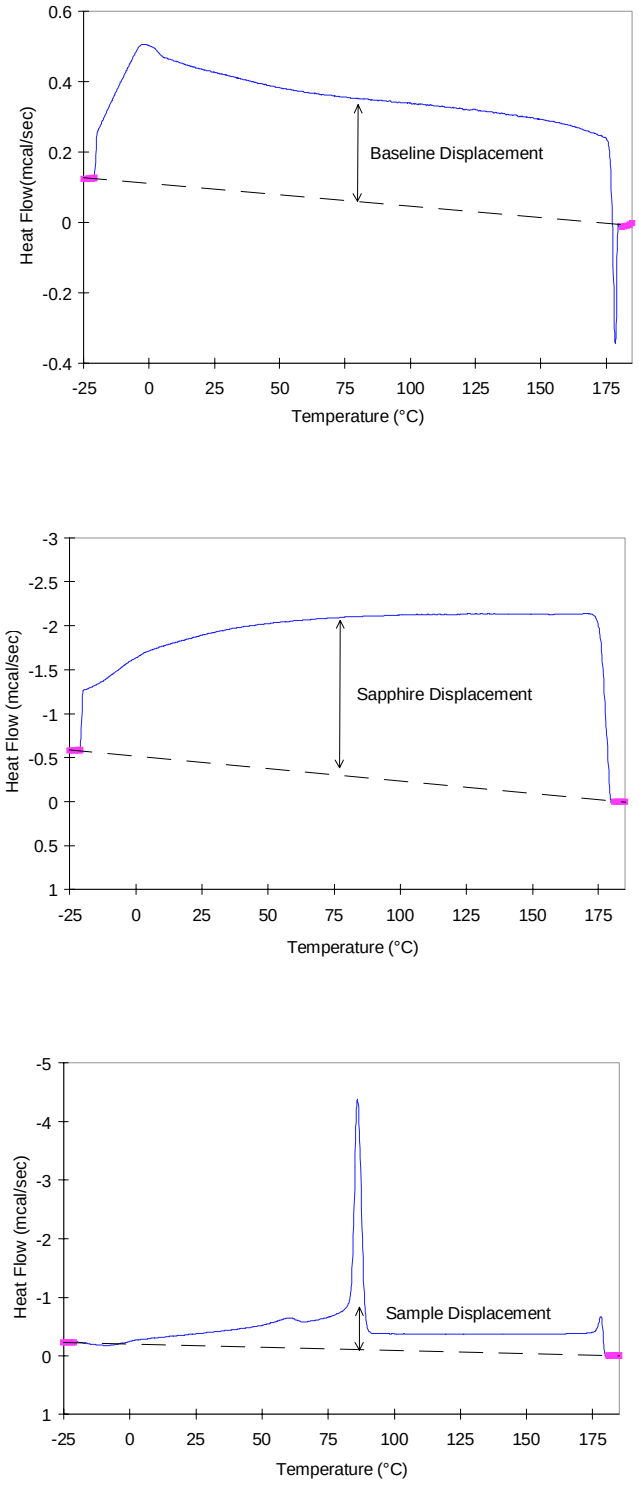

Figure 1 The displacements corresponding to the baseline, sapphire and the copolymer, EB-912 during cooling from the melt (180°C) at 20°C/min.

where $D_p^{sapphire}$, D_p^{sample} = effective displacements of sapphire and sample respectively

$W_{sapphire}$, W_{sample} = weights of sapphire and sample (in mg) respectively, and

$C_p^{sapphire}$ = the absolute heat capacity of sapphire (from literature[14]).

The absolute heat capacities calculated using this expression for the sample in our example are shown in Figure 2.

Step 4. The partial areas as a function of temperature were estimated from the areas under the C_p curves. These values were then divided by the appropriate factors to account for the conversion in units from mcal/sec to J/deg.mole, to yield approximate values for the degrees of crystallinity as a function of temperature, $\chi_c(T)$. It is worthwhile to mention that the $\chi_c(T)$ values thus estimated are only approximate since they are based on a linear baseline under the C_p curve.

Step 5. The C_p baselines for the samples were constructed from the approximate crystallinity values using the following relationship. The C_p's of the crystal fractions were obtained from the literature.[14]

(3) $$C_p^{sample} = C_p^{Amorphous} \times (1 - \chi_c(T)) + C_p^{Crystal} \times \chi_c(T)$$

The C_p baseline curve (also shown in Figure 2) was then subtracted from the absolute heat capacities estimated in Step 3, to yield the "final" heat capacities as shown in Figure 2. The final C_p directly corresponds to the amount of amorphous material transformed to the crystalline state, at a specified temperature.

Step 6. The partial areas as a function of temperature were calculated from the final heat capacity curve to yield the degrees of crystallinity at any temperature. The crystallinities as a function of temperature for all copolymers are shown in Chapter 5.

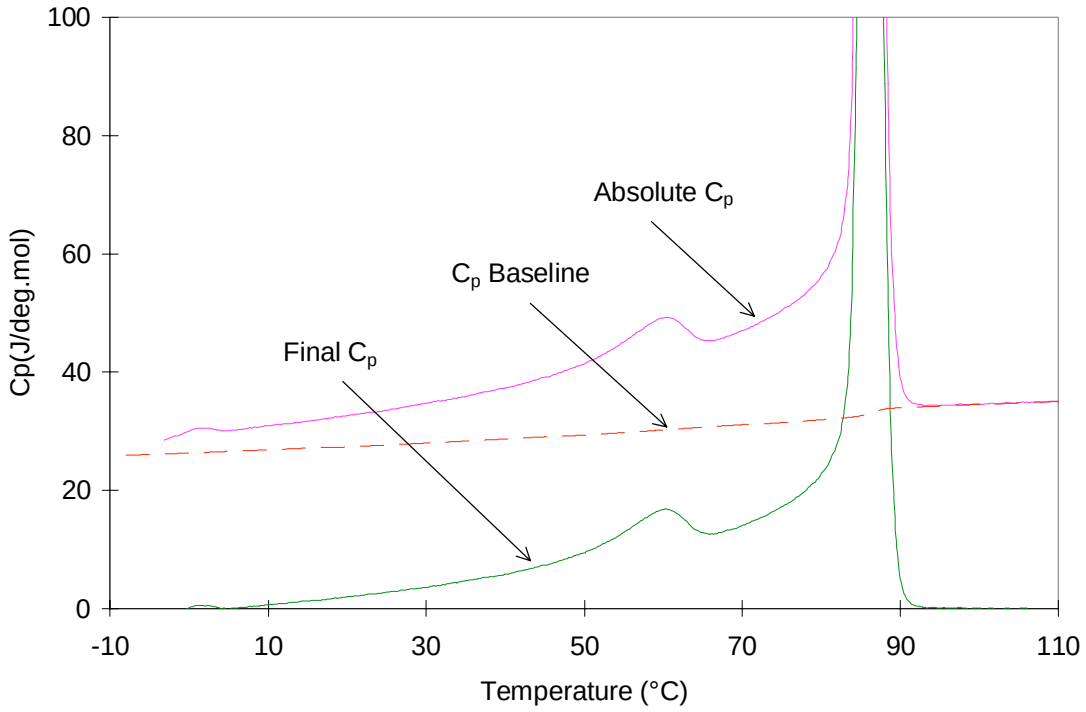

Figure 2 Absolute heat capacities, the C_p baseline and the "final" heat capacities for EB-912 cooled from the melt at 20°C/min.

3.3.2 Deconvolution of Low Endotherm Areas

The ethylene/α-olefin copolymers with varying branch concentrations were crystallized at different temperatures (T_x), for times ranging from 10^0 - 10^6 min. The melting traces collected after different crystallization times (t_x) (at any T_x) exhibit a low and a high melting endotherm. The heats of fusion corresponding to the low endotherms were determined by a deconvolution process involving curve fitting. The procedure adopted for this purpose is outlined below.

Step 1. For a set of isothermal crystallization experiments at a specified T_x, the corrected heating trace of the sample directly quenched from the melt, i.e., $t_x = 0$, was fit by an appropriate number of Gaussian peaks. [The DSC scan of the quenched sample does not exhibit a low endotherm]. To minimize the subjectivity of the curve-fitting procedure, the number of peaks and the integration range chosen were maintained constant within each series. It is also noted that the peaks do not bear any physical significance, but merely serve as mathematical tools that enable the calculation of the area under a curve, within a given range of temperatures. An example is shown in Figure 3(a) for EB-883 quenched from the melt (160°C) to -20°C, and re-heated immediately.

Step 2. Using the fitted curve of the quenched sample as the basis, the heating traces of the samples crystallized for various times at T_x were modeled by incorporating an extra peak to aptly represent the presence of a low endotherm. The evolution of the low endotherm with crystallization time was accounted for by increasing the magnitude of the extra peak and shifting it to higher temperatures, while maintaining the integrity of the other peaks. The position and area of the extra peak correspond to the position and area of the evolving low endotherm, respectively. Example of the results of curve fitting are depicted in Figure 3(b) and (c), for EB-883 crystallized at $T_x = 40$°C for different times.

Step 3. The relative areas were subsequently converted into the absolute contribution of the low endotherm to the total heat of fusion. Such an analysis also provides a means of evaluating the total heats of fusion of the melting traces. It is important to mention that

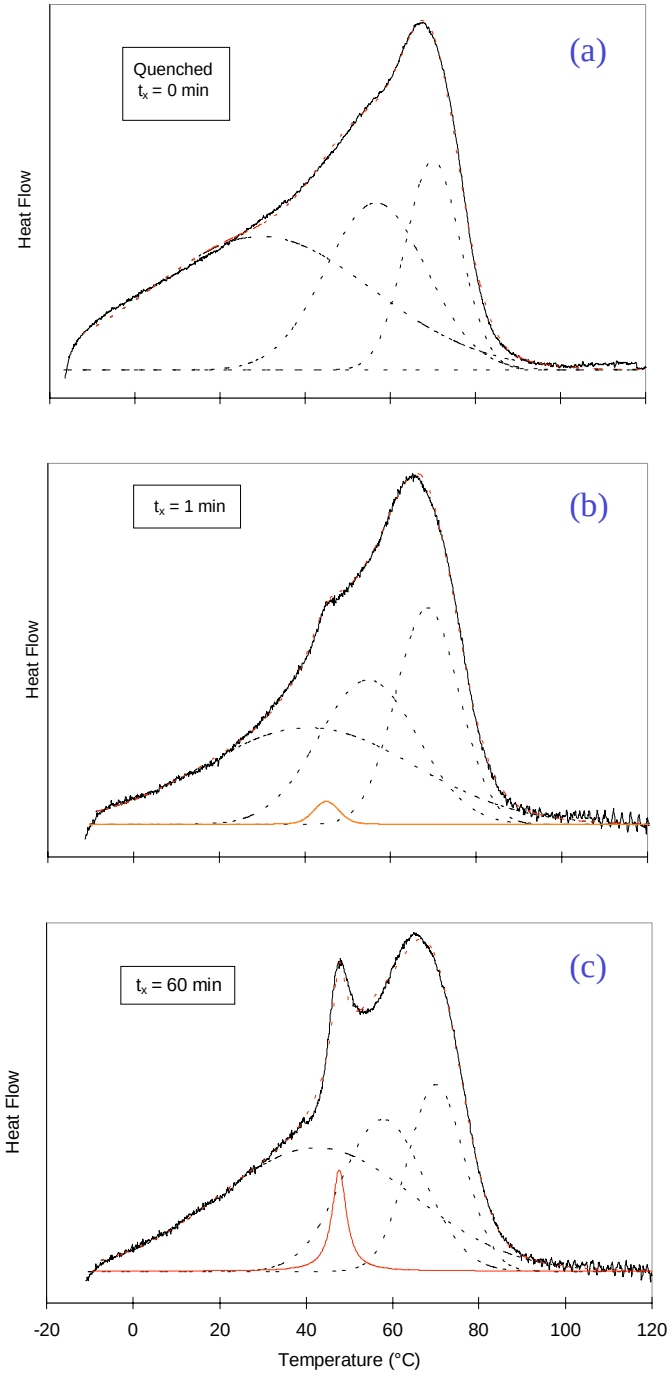

Figure 3 Evolution of the low endotherm for EB-883 quenched from the melt (160°C) to -20°C and subsequently crystallized at T_x = 40°C for various times. The Gaussian peaks used in the deconvolution are also shown (black lines). The red curve represents the low endotherm. (a) Quenched, (b) t_x = 1 min, (c) t_x = 60 min.

this procedure is meaningful only because the total area of the scan, within a given range, remains invariant with crystallization time.

3.3.3 Degree of Crystallinity

The crystallinities of the copolymers were evaluated using the relationship given by Equation (1) also shown below,

$$\chi_c = \frac{\Delta H_{obsd}}{\Delta H_0}$$

where ΔH_{obsd} = the experimentally observed heat of fusion, and

ΔH_0 = the heat of fusion of purely crystalline linear PE.

A value of ΔH_0 = 69 cal/g[12,13] was used in the evaluation of the crystallinities of the ethylene/α-olefin copolymers. There are however, a few related aspects that need to be considered when this value is applied to the copolymers in the present study.

1. The value of ΔH_0 = 69 cal/g is the theoretical heat of fusion of a purely crystalline LPE sample, all of whose crystals are of the orthorhombic unit cell structure. However, the presence of another crystal form (in addition to the usual orthorhombic one) in the copolymers is clearly demonstrated from the infrared experiments (Chapter 7). The steric stresses at the lamellar surfaces arising from the lack of regular chain folding and the overcrowding in the amorphous regions from the accumulation of branched units hamper the growth of these crystals in the lateral directions. In addition, their thickness is limited by the relatively short lengths of the crystallizable ethylene sequences available in the inter-lamellar amorphous regions. These facts are further reflected in the lower melting temperature of the secondary crystals and their

associated features (bridge-like structures between the lamellae) in the Atomic Force Micrographs. In accordance with these results, recent results from Monte Carlo simulations indicate a lower density (lower co-ordination of the ethylene sequences) for the crystals in similar ethylene/α-olefin copolymers[15]. It is also known from the literature[16] that the density of the orthorhombic crystals is higher than that of the other crystal modifications suggested for the secondary crystals. Accordingly, the heats of fusion of the orthorhombic crystals must also be higher than the latter type of crystals. Therefore, the use of the value, ΔH_0 = 69 cal/g for the copolymer crystals may be a significant approximation, especially for the highly branched samples.

2. The theoretical heat of fusion, ΔH_0 for LPE is defined at its equilibrium melting temperature (~145°C). However, this value is applied to the copolymers that melt over a wide range of temperatures extending to as low as their glass transition temperatures (T_g). In order to remedy this discrepancy, the theoretical heat of fusion must be evaluated at the different melting temperatures of the copolymers, using the heat capacities of the melt and the crystal phases. The C_p's of the copolymers in their melt state have been evaluated in the present study and are found to exactly match those for LPE (in its melt). However, the heat capacities of the copolymers in the crystalline state are not easily obtained due to the fact that the melting of copolymer crystals begins right above their T_g and extends over a large range of temperatures.

3. The penalty in the equilibrium value of heat of fusion arises from the surface enthalpic contributions. This deviation from the equilibrium value is particularly significant for the more highly branched copolymers since such copolymers exhibit an ethylene sequence distribution centered at a low value and crystallize predominantly in the fringed-micellar form. Such a crystalline morphology is characterized by a very large specific surface. Therefore, the surface enthalpy and the crystallizable segment length in the copolymers must

be independently determined in the entire temperature range examined. However, this information is not presently available in the literature.

Therefore, it must be realized that the degrees of crystallinity determined in the present study are subject to some uncertainty.

3.4 Fourier Transform Infrared Spectroscopy (FTIR)

The degree of crystallinity and, indirectly, some information about chain conformation, packing and crystal structure were examined via Fourier Transform Infrared Spectroscopy. The experiments were carried out on a BioRad FTS-40A FTIR Spectrometer equipped with a liquid nitrogen cooled detector, and a hot stage connected to a temperature controller. The spectra were collected in the range between 400 and 4000cm^{-1} with a spectral resolution of 2 cm^{-1}. Every spectrum collected was an average of 64 scans.

The samples used were in the form of ~ 30-50 μm thick films. They were prepared by pressing a pre-pressed film between two flat aluminum plates. The thin films thus obtained were further treated in the following manner in order to erase the surface features that were present originally. [These features were developed on pressing the films between either Teflon films or metal plates in the original sample preparation]. They were placed on a clean glass cover slip and heated gradually until they just melt. Then they were immediately quenched into liquid nitrogen. This procedure yielded thin films devoid of previously developed surface features as well as voids, cracks and other such irregularities. Such features, if present, could lead to artifacts and misleading conclusions in the infrared experiments. The thin films thus obtained were held between two clean KBr plates and were subsequently placed inside a modified sample cell in the IR chamber, which was continuously purged with nitrogen gas. The sample was also directly in contact with a thermocouple that measured the temperature of the sample within ±1°C. The first spectrum was collected approximately 20 minutes after placing the sample inside the chamber. This time served to remove any residual moisture and/or

carbon dioxide that could lead to spurious and undesired peaks in the infrared spectrum of the sample.

The experiments were designed primarily to examine the influence of branch content and thermal history (cooling rate) on the crystallization and melting behaviors of the copolymers. Three sets of experiments were performed. First, the samples were heated from 25°C to the melt (160°C) at a rate of ~ 1.5°C/min. Infrared spectra were collected at intervals of 5°C after ensuring that the sample had attained thermal equilibrium at that temperature. Since each spectrum was an average of 64 scans, the time taken for data collection at each temperature was 64 seconds. Care was taken to ensure that the sample remained within ±1°C of the temperature at which data was obtained, throughout the time span of collection. As the temperature approached the melting temperature of the sample, spectra were obtained at 2°C intervals, in order to effectively follow the melting process.

In the second set of experiments, the samples were cooled down from the melt (160°C) to 25°C (immediately after the heating experiments) at a cooling rate of ~1.5°C/min. Sample spectra were collected following a similar procedure as adopted for the heating cycle mentioned above. Then, the samples were held at room temperature (~23°C) in a nitrogen atmosphere for ~12 hours, after which a second heating cycle was performed. It is to be noted that the spectra collected during the first heating cycle are associated with a quenched sample; whereas those from the second heating cycle are obtained from a sample that was slowly cooled from the melt and subsequently isothermally annealed at room temperature (~ 23°C) for about 12 hours.

Prior to collecting the infrared spectra of the copolymers, background spectra were obtained at all the test temperatures, during both heating and cooling cycles. The background at a given temperature was subtracted from the sample scan at that temperature, before analyzing the spectrum.

3.5 Atomic Force Microscopy (AFM)

3.5.1 Experimental

The morphology of the copolymers was studied as a function of branch content via Atomic Force Microscopy (AFM). These experiments were performed on a Digital Instruments Dimension 3000 Microscope attached to a Nanoscope IIIa controller. The experiments were carried out in the tapping mode with Tapping Etched Silicon Probe™ (TESP) cantilevers. The thin films prepared for the infrared studies were suitable for use in the AFM experiments. It was ensured that these films are devoid of previously formed surface features as well as irregularities. A brief background of the significant aspects of this technique is given below. This review also justifies the choice of the tapping mode employed in the present study.

3.5.2 Theory

Since the early seventeenth century, optical microscopes (OM) have been widely used for imaging and studying the morphology of materials on a microscale. Although this technique has been highly successful for the purposes mentioned above, it has a few limitations, as listed below.

- It does not provide information on the size (in the micrometer or below range) of features in a direction normal to the plane of the sample surface, and
- Its resolution is limited by the wavelength of light used (diffraction limit).

The next major development in the study of surface morphologies was the introduction of Scanning Electron Microscopes (SEM) in the 1940s. The largest advantage of this technique over OM is the fact that the optical properties of the samples were no longer significant, since an electron beam instead of a photon source is used to

image the sample surface. However, SEM suffers from the same limitation as OM with respect to the size of features perpendicular to the sample surface plane[17].

Scanning Probe Microscopy (SPM) became known as a new tool for surface imaging in the early 1980s. This technique uses a sharp probe whose tip is on the order of a few nanometers radius of curvature and has a very steep sidewall angle. The sharp probe scans over the sample surface at spacings within a nanometer from the surface. This results in resolutions of the order of 0.1 to 3 nm in the *x* and *y* directions, and 0.01 nm in the *z* direction. Thus, SPM is capable of providing three-dimensional measurements with a higher resolution than possible with both OM and SEM.

Scanning Tunneling Microscopy (STM) was one of the earliest known modes of SPM.[17] It uses a sharp conducting tip that is scanned over the surface of a conducting sample. Although this technique is an excellent means of examining surfaces, its application is restricted to conducting samples. This led to the introduction of Atomic Force Microscopy (AFM) in 1989 as an alternative method that is applicable to non-conducting samples as well[17]. The probe in AFM is placed at the end of a cantilever with a low spring constant. This technique can be performed in a number of modes such as contact, tapping, lift etc. In the contact mode, a very small force in the range of 9 to 10 Newtons is applied to the cantilever, which is in contact with the sample surface. Such low magnitudes of force employed are meant to prevent damage to the samples. This force also helps to maintain the spacing between the probe and the sample at a constant value. The contact mode however suffers from the following limitations.

- The force employed is large enough to damage some sensitive surfaces like those of biological samples and most polymeric materials
- The friction between the tip and the sample gives rise to shear forces that can deform the samples
- It is not possible to examine surfaces with loosely bound species, since they are displaced by the probe

These problems have been overcome with the introduction of the tapping mode, where the probe (mounted on the cantilever) is oscillated at a frequency close to its resonance value. The amplitude of oscillations is monitored by the system. Then the tip

is lowered by the *z* component of a piezoelectric scanner[18] until it just touches the sample surface. Contact between the tip and the sample surface causes a decrease in the amplitude of oscillations. The scanner adjusts the height of the tip to suit the distance between the tip and the surface, as surface features (changes in heights etc.) are encountered. Thus, it becomes possible to examine the surfaces of highly sensitive species without the undue application of forces that may alter the existing surface features.

While in the tapping mode, it is possible to monitor the phase lag between the cantilever oscillation and the signal received by the piezoelectric scanner. This extension of the tapping mode is referred to as phase imaging. It is very sensitive to variations in properties such as composition, surface hardness, adhesion and viscoelasticity, but not to surface height variations. Therefore it permits the distinction of fine features that may be obscured by rough surface scanning. All the images of the copolymers presented in Chapter 6 are phase images of the type discussed above. It is noted that the phase contrast represented by the color changes in the micrographs is a manifestation of the differences in molecular packing and modulus (hardness) in the samples. Regions of different moduli within the sample result in considerably different responses in the output signal received from the oscillations of the tip. The differences arise mainly due to the fact that the oscillating tip plunges to a greater depth when a softer (low modulus) region is encountered. Regions of relatively higher moduli within the sample appear as bright regions in the micrographs, whereas the softer regions between the crystallites appear as dark areas.

Thus, it is clear that the tapping mode is far superior in preserving the integrity of the sample and providing information on surface features than the contact mode. Use of the contact method would be particularly detrimental when studying the most highly branched copolymers. These materials are very soft and are highly susceptible to deformation by even minor applications of force, let alone the force due to the pushing of the probe against the sample surface. Then, the choice of the tapping mode for the copolymers studied here is justified.

[1] K. Ziegler, E. Holzkamp, H. Breil and H. Martin, *Angew. Chem*., **67**, 541 (1955)
[2] G. Natta, P. Pino, P. Corradini, F. Danusso, E. Mantica, G. Mazzanti and G. Moraglio, *J. Am. Chem. Soc.*, **77**, 1708 (1955)
[3] G. Natta, *J. Polym. Sci.*, **16**, 143 (1955)
[4] J. C. Randall, *J. Polym. Sci., Polym. Phys. Ed.*, **14**, 1693 (1976)
[5] D. E. Axelson, L. Mandelkern and G. C. Levy, *Macromolecules*, **10**, 557 (1977)
[6] D. E. Axelson, G. C. Levy and L. Mandelkern, *Macromolecules*, **12**, 41 (1979)
[7] J. C. Randall, *J. Polym. Sci., Polym. Phys. Ed.*, **11**, 275 (1973)
[8] J. J. Dechter and L. Mandelkern, *J. Polym. Sci., Polym. Phys. Ed.*, **18**, 1955 (1980)
[9] F. Cavagna, *Macromolecules*, **14**, 215 (1981)
[10] J. C. Randall, *J. Appl. Polym. Sci.*, **22**, 585 (1978)
[11] F. A. Bovey, "*Nuclear Magnetic Resonance Spectroscopy*", Academic Press, New York, 1988
[12] P. J. Flory and A. Vrij, *J. Am. Chem. Soc.*, **85**, 3548 (1963)
[13] F. A. Quinn, Jr. and L. Mandelkern, *J. Am. Chem. Soc.*, **80**, 3178 (1958)
[14] B. Wunderlich, *The Athas Data Bank on Heat Capacities of Polymers, Pure and Applied Chem.*, **67**, 1919 (1995)
[15] V. B. F. Mathot, R. L. Scherrenberg and T. F. J. Pijpers, *Polymer*, **39**, 4542 (1998)
[16] B. Wunderlich, *"Macromolecular Physics*", Vol. 3, Academic, New York (1980)
[17] Information from the Digital Instruments Homepage: http://www.di.com/
[18] D. R. Baselt and J. D. Baldeschwieler, *Rev. Sci. Instr.*, **64**, 908 (1993)